ACS Photonics

Article

pubs.acs.org/journal/apchd5

Plasmons in Cylindrical 2D Materials as a Platform for Nanophotonic Circuits

Irati Soto Lamata,[†,‡] Pablo Alonso-González,[‡] Rainer Hillenbrand,[§,∥] and Alexey Yu. Nikitin*[,‡,§]

[†]Tecnun (University of Navarra), 20018 Donostia-San Sebastian, Spain

[‡]CIC nanoGUNE, 20018 Donostia-San Sebastian, Spain

[§]IKERBASQUE Basque Foundation for Science, 48011 Bilbao, Spain

[∥]CIC nanoGUNE and UPV/EHU, 20018 Donostia-San Sebastian, Spain

Supporting Information

ABSTRACT: Materials of reduced dimensionality (graphene, thin BN layers, etc.) open new pathways to control electromagnetic fields at the nanoscale by the excitation of tunable and highly confined propagating surface plasmon-polaritons. However, compressing and channeling of plasmons along 2D ribbons suffer from scattering at edges. The concept of using edgeless 2D rolled-up sheets, in particular carbon nanotubes (CNTs), for potential integration into plasmonic nanocircuits has not been explored yet. Apart from supporting plasmons with extremely short wavelengths (providing thus a strong light compression), the optical properties of CNTs are highly sensitive to the environment and external fields. Here, we study the launching and propagation of CNT plasmons in different key plasmonic structures, which include both coupled CNT waveguides and coupled CNT−graphene resonators. We also show an efficient way of launching and phase control of propagating graphene plasmons with the help of a CNT antenna. Combining CNTs with graphene could become a promising route toward ultracompact plasmon circuitry at the nanoscale.

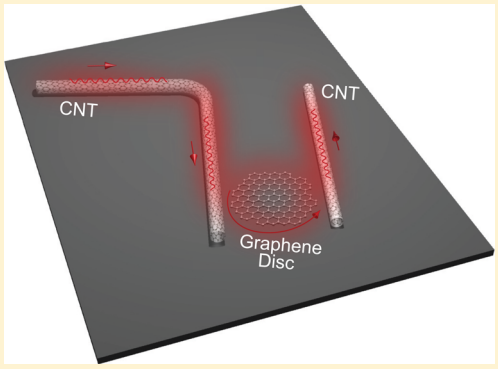

KEYWORDS: *carbon nanotube, graphene, plasmon*

Recently, propagating short-wavelength graphene plasmons (GPs) have shown their strong potential for the development of mid-infrared (IR) and terahertz (THz) plasmonics.[1−12] The main advantages of graphene over metals consist in its exceptional thinness and an efficient electrostatic control of GPs. Moreover, in an infinitely extended graphene sheet, plasmons have an extremely short wavelength, λ_p, 10 to 100 times smaller than the corresponding photon wavelength in free space, λ, which shows their strong confinement to the graphene sheet.

The degree of confinement of the plasmonic fields can be further increased by a reduction of the dimensionality. For example, in graphene ribbons of width w, comparable with the GP decay length in the vertical direction, $w \approx L_z \approx 1/\mathrm{Re}(k_p) = \lambda_p/2\pi$, plasmons have significantly shorter wavelength compared to plasmons in an infinite graphene sheet.[13] In practice, however, the graphene edges (while providing higher local density of photonic states) introduce imperfections (electrically inactive regions, etc.) and thus undesired losses.[14]

Here we demonstrate that in order to keep the degree of confinement and avoid plasmonic scattering at edges, the graphene (or another 2D material) ribbon could be rolled into a cylinder. For example, carbon nanotubes (CNTs), naturally rolled carbon monolayers (systems with a rich physics and interesting applications in electronics, optoelectronics, and photonics[15,16]), can perform as natural edge-free plasmonic waveguides of reduced dimensionality. Besides their ability to confine and guide IR plasmons, cylindrical 2D sheets (C2DS) could be further combined with graphene-plasmonic elements such as discs, ribbons, etc. C2DSs could thus have promising application potential for building integrated tunable plasmonic nanodevices.

We study the excitation and propagation of plasmons in C2DS and combined C2DS−graphene structures by conducting full-wave numerical simulations. As an example of C2DS, we consider single-walled CNTs, in which the existence of plasmons is known,[10,17−22] but not yet explored for nanocircuit applications. We perform the calculations in the mid-IR spectral range (from 8 to 12 μm wavelength) because of potentially interesting near-field microscopy experiments.[1] We also illustrate energy transfer from one CNT to another via both direct CNT plasmon (CNTP) coupling and by using a graphene disc resonator. Finally, we utilize a finite-length CNT as an antenna for launching propagating GPs into a graphene sheet.

In order to model the optical properties of CNTs, we do not take into account quantum effects, but instead, for simplicity,

Received: October 8, 2014

DOI: 10.1021/ph500377u
ACS Photonics XXXX, XXX, XXX−XXX

use the standard model of the conductivity for graphene (local random phase approximation with the dominating Drude term[9,23,24]). This model has been shown to be a good estimation for the optical properties of CNTs with sufficiently large radii and for plasmon energies less than the Fermi level.[10] Having in mind these restrictions, we will study here only large-diameter CNTs (with diameters $d \approx 10$ nm). We expect, however, usual CNTs ($d \approx 1$ nm) to show similar optical behavior, but supporting plasmons with shorter wavelengths. Notice that although large-diameter single-walled CNTs ($d > 3$ nm) are not commonly used, the technique for their fabrication is known,[25−28] and therefore CNTs of diameters considered here are realistic.

Throughout the whole article we consider a Fermi level of $E_F = 0.3$ eV and a charge carrier relaxation time of $\tau = 0.5$ ps (corresponding to a mobility of $\mu_e = 1.67 \times 10^4$ cm^2 V^{-1} s^{-1}) at room temperature, $T = 300$ K. These parameters are typical for graphene sheets in which graphene plasmons are observed in the IR.[1,2,29] Since in this paper we consider graphene structures where the separation between the Fermi energy and the Dirac point is much larger than temperature and relaxation energy, we neglect in our macroscopic electrodynamic analysis the microscopic details of the edges.[13]

We first study the dispersion relation of CNTPs and compare it to that of plasmonic modes in either infinite graphene sheets, graphene ribbons, or graphene edges. The ribbon width w has been chosen to correspond to the "unrolled" CNT, i.e., $w = \pi d$, where d is the diameter of the CNT. We calculate the modes by solving the eigenvalue problem for graphene structures in free space (for simplicity).

Figure 1 illustrates both the dispersion and spatial distribution of the absolute value of the electric field, |**E**|, of the plasmonic modes. Figure 1a shows the momentum of the plasmonic modes, k_p,[30] normalized to the free-space wavevector

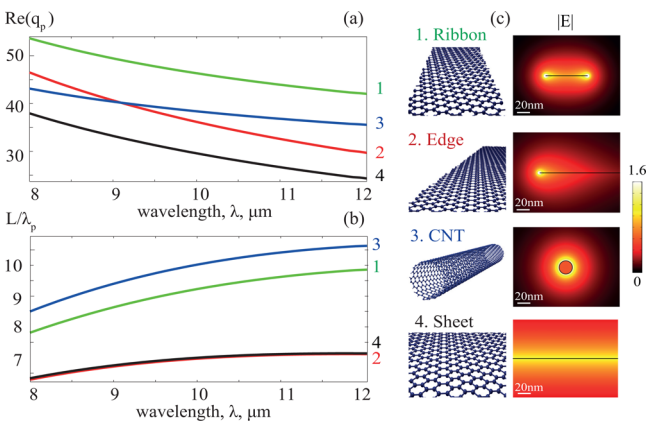

Figure 1. Comparison of plasmonic modes in different graphene structures: ribbon (green curves), edge (red curves), single-wall CNT (blue curves), and infinite graphene sheet (black curves). (a) Plasmon momentum, q_p, and (b) propagation length, L_p, are shown as a function of the wavelength. (c) Schematic of the structures and the spatial distribution of |**E**| at the corresponding points in the dispersion curves marked by the numbers. In each case the fields are normalized to their values at the distance 5 nm away from the surface (cases "3" and "4") or from the edge (cases "1" and "2"), respectively. The diameter of the nanotube and the width of the ribbon are $d = 20$ nm, $w = 62.8$ nm, respectively. The parameters for the conductivity for all structures are Fermi energy, $E_F = 0.3$ eV, relaxation time of charge carriers, $\tau = 0.5$ ps, and temperature, $T = 300$ K.

$k_0 = 2\pi/\lambda$ as a function of free-space wavelength λ. One can observe that the normalized momentum $q_p = k_p/k_0$ in an infinite graphene sheet (black curve) is lower than that of the plasmonic modes in all the shown structures, while the plasmonic mode of the ribbon has the highest q_p (green curve). Notice that for the ribbon only the fundamental mode with antisymmetric vertical electric field distribution is considered. This mode appears due to the coupling of the plasmons propagating along the opposite ribbon's edges.[13] Interestingly, the dispersion curves for CNTPs (blue curve) and edge plasmons (red curve) intersect so that q_p of CNTPs is larger than q_p of edge plasmons for wavelengths longer than $\lambda = 9.2$ μm for the shown parameters. Another remarkable observation is that the propagation length, L_p, of plasmons in the infinite graphene sheet and that of edge plasmons coincide when represented in units of the plasmon wavelength λ_p (Figure 1b). This is due to the fact that the complex-valued momentum of an edge plasmon, q_{pe}, linearly scales with that of plasmons in the infinite graphene monolayer, q_{p0}, so that $q_{pe} = 1.23q_{p0}$. Most importantly, Figure 1b shows that CNTPs exhibit the highest relative propagation length, L_p/λ_p, among all the considered structures, even compared to plasmons in the infinite graphene sheet (note that the Fermi level and mobility are the same for all structures). Apart from the strong localization of electromagnetic fields, a longer propagation length is another key advantage of CNTs over graphene ribbons for using them as IR plasmonic waveguides with ultrashort wavelengths.

In practice, both graphene and CNT structures are placed onto a substrate. Therefore, we next study the influence of the substrate on the properties of CNTPs. In the inset to Figure 2a one can see that q_p linearly increases with the increase of the dielectric permittivity of the substrate, ε, similarly to GPs in an infinite graphene monolayer, where $q_{p0} \approx q_0(1 + \varepsilon)/2$, with q_0 being the momentum of GP in an infinite free-standing monolayer. The field distributions shown to the right of Figure 2a indicate that for higher values of ε the field of the mode is enhanced in the vicinity of the contact between the CNT and the substrate. Such a field concentration in CNTs could be used for plasmonic sensing applications,[12] especially in cases when a tiny quantity of material needs to be tested.

We next study the influence of the CNT diameter d on the plasmon dispersion (Figure 2b). We find that the momentum of CNTPs is higher for thinner nanotubes and monotonically increases with the decrease of d, as follows from the inset to Figure 2b. The momentum increase leads to a higher localization of the CNTPs, as seen from the electric field distributions shown to the right of Figure 2b. While the plasmons for thinner CNTs become more confined, the momentum mismatch between them and free-space radiation gradually increases.

In order to compensate the large momentum mismatch, a localized source (for example, a dipole) with a size smaller than the CNTP wavelength can be used. Such a source provides the necessary momentum components for launching CNTPs in analogy with the launching of GPs.[6,7] Figure 2c visualizes the propagation of CNTP launched by a vertical electric dipole. The spacing between the fringes of the same color in the distribution of the vertical electric field E_z along the CNT gives the CNTP wavelength, $\lambda_p = 260$ nm, which coincides with the value from the eigenmode solution, $\lambda_p = \lambda/\mathrm{Re}(q_p)$, thus clearly revealing that the plasmon propagates along the CNT.

DOI: 10.1021/ph500377u
ACS Photonics XXXX, XXX, XXX−XXX

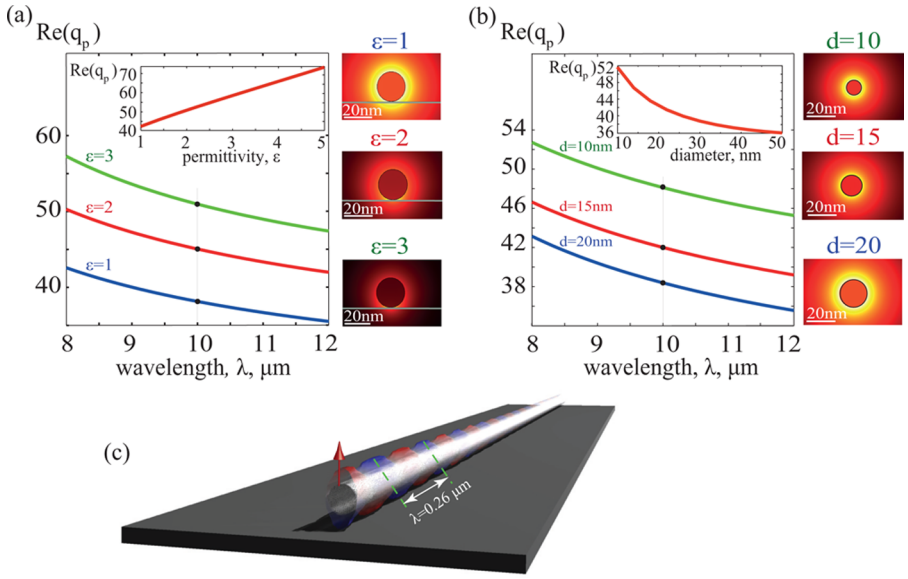

Figure 2. Influence of the substrate and the size of the CNT on the momentum of the CNTPs, q_p. (a) q_p as a function of the wavelength λ for CNT on different substrates. The CNT diameter is d = 20 nm. Inset to (a): q_p as a function of the dielectric permittivity of the substrate at λ = 10 μm. (b) q_p as a function of λ for CNT of different diameters d in free space. Inset to (b): q_p as a function of d at λ = 10 μm. The images located to the right from each panel show the distribution of the absolute value of the electric field at λ = 10 μm. (c) Spatial distribution of the vertical component of the electric field created by a point dipole separated from the CNT by the distance of 5 nm. The parameters of the conductivity for both panels are the same as in Figure 1.

Apart from potential applications related to guiding of the plasmons and plasmonic sensing, CNTs can be used for spatial modulation and power division of the electromagnetic fields. We further consider the possibility of building up an efficient directional coupler[31−33] by using two parallel-aligned CNTs. Figure 3 illustrates the plasmonic coupling between two CNTs, which are closely brought together (we take the separation distance of 10 nm, to provide a high coupling efficiency; see details in the Supporting Information). The plasmon is excited by a vertical dipole placed 5 nm away from the surface of the upper CNT (nanotube A) and 1 μm away from the beginning of the lower CNT (nanotube B) (the dipole is sketched by a vertical red arrow in the schematics of Figure 3). In Figure 3a and b, which show the spatial distribution of |**E**| and Re(E_z), respectively, one observes a beating pattern (a set of alternating minima and maxima in the field in each nanotube) typical for coupled waveguides.[31−33] The beating originates from (i) the hybridization of the plasmonic modes in the coupled CNT waveguides[34,35] and (ii) consecutive energy transfer between these modes. Such a waveguide system does not allow guiding SPPs along nanotube B, since it always returns back to nanotube A. However, if nanotube A is cut at the point of its field minimum, SPPs can be totally transferred from nanotube A to nanotube B, as demonstrated in Figure 3c and d. This observation confirms that coupled CNTs indeed can be used as coupled plasmonic waveguides, spatial shifters, and splitters in the IR.

The above results are encouraging for the development of other CNT-based plasmonic components. For instance, one can design a resonator composed of a CNT and a graphene disc supporting an edge plasmonic mode. This configuration is similar to a waveguide-ring resonator, widely used in different plasmonic structures.[36,37] The schematic of the device is shown in Figure 4a (left). A vertical dipole launches plasmons on a CNT, and they propagate toward a graphene disc, where they further couple to the edge plasmons of the disc. The absorption

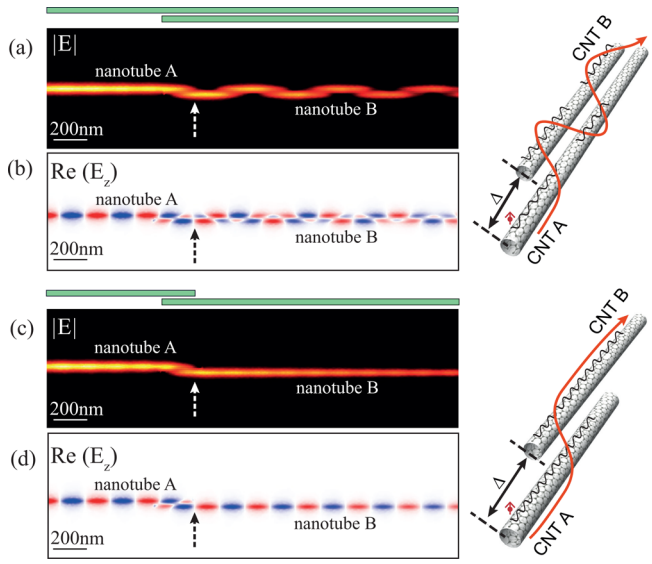

Figure 3. Spatial distribution of |**E**| and Re(E_z) for two parallel coupled CNTs. The diameter of CNTs is d = 20 nm; the separation between them is 10 nm. The CNTP is launched along CNT A by a point source placed Δ = 1 μm away from the beginning of CNT B. The free-space wavelength is 10 μm. (a, b) Infinitely long coupler. (c, d) Cut coupler, with the length of the coupling part 200 nm. The dashed arrows in (a) and (b) indicate the position of the field minimum in CNT A, while in (c) and (d) they show the termination of CNT A. The upper schematics show the exact positions of the CNTs (top view). The right schematics illustrate the geometry of the structures and propagation of the CNTPs (red arrows represent the power flux). The parameters of the CNT conductivity for all panels are the same as in Figure 1.

of the graphene disc A_{disc} (dominated by the edge GPs) is plotted in Figure 4b as a function of the wavelength (blue curve). A_{disc} is normalized to the absorption by an infinite

DOI: 10.1021/ph500377u
ACS Photonics XXXX, XXX, XXX−XXX

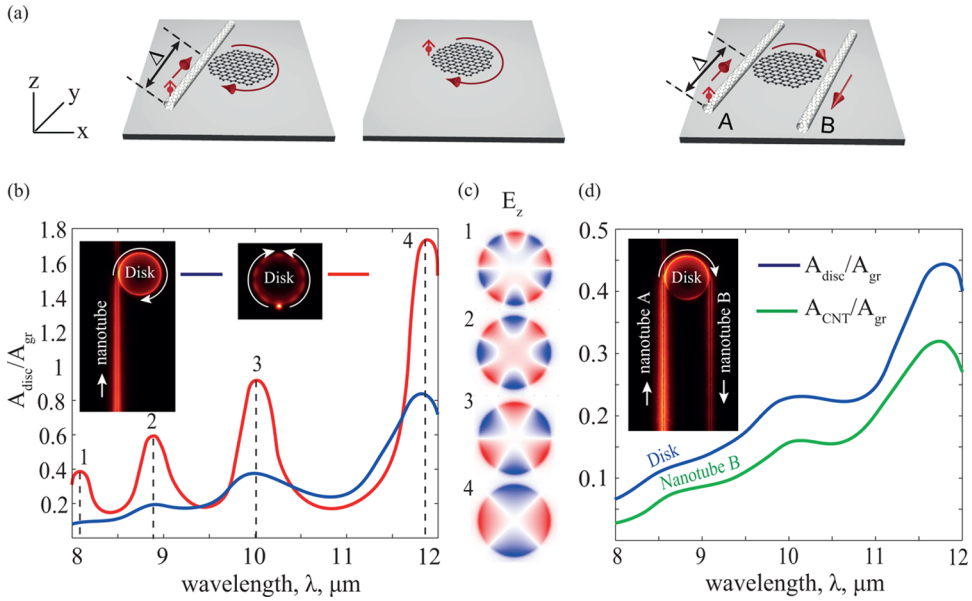

Figure 4. Coupling of CNTPs via a graphene disc plasmonic resonator. The CNTP is excited by a dipole placed 1 μm away from the point of the closest CNT−disc separation (which is 5 nm). The disc diameter is 300 nm. (a) Schematics of the structures. (b) Normalized absorption in the graphene disc A_{disc}/A_{gr} as a function of the free-space wavelength λ. Red curve: Plasmons are excited by a dipole. Blue curve: Plasmons are excited by the CNT. Insets to (b): Spatial distribution of |**E**| for the cases of the excitation by CNTPs or a point source for λ = 8.08 μm (the first peak). (c) Instant snapshots of Re(E_z) at the surface of the graphene disc. The numeric labels correspond to the peaks in the red and blue curves of panel (b). (d) Normalized absorption in the graphene disc A_{disc}/A_{gr} (blue curve) and in the CNT B A_{CNT}/A_{gr} (green curve) as a function of λ. Insets to (d): Spatial distribution of |**E**| for λ = 11.76 μm. The parameters of the conductivity for both panels are the same as in Figure 1.

graphene sheet, A_{gr}, when the vertical point source is placed 5 nm away from it. The separation between the disc and the CNT (10 nm) has been chosen to provide an optimal coupling in the vicinity of the wavelength, λ = 10 μm (see details in the Supporting Information). One can observe a set of maxima corresponding to the different resonance orders m, according to $P \approx m\lambda_{pe}$, i.e., m times the edge plasmon wavelength λ_{pe} along the perimeter $P = \pi D$ (with D being the diameter of the disc). Note that the resonance condition predicts equidistant resonance positions when expressed as a function of λ_{pe}. However, the distances between the different maxima in Figure 4b are not the same. This is due to both the nonlinear dispersion of the edge graphene plasmon, $\lambda_{pe}(\lambda)$, and the radiation losses being especially relevant for lower-order modes. Snapshots of Re(E_z) at the resonance maxima of A_{disc} are shown in Figure 4c. For each maximum, the snapshots show different numbers of alternating red and blue fringes. The distance between two fringes of the same color corresponds to λ_{pe} and their number m counts from 2 to 5. This is fully consistent with the above resonant condition for the disc diameter of D = 300 nm. Indeed, according to Figure 1a (red curve), the momentum of the edge plasmon, q_{pe}, ranges from 46.5 to 29.7, thus yielding values of P/λ_{pe} from 2.3 to 5.5.

For comparison, the red curve in Figure 4b shows the absorption in an isolated disc, where edge plasmons are excited by a vertical dipole located 5 nm away from the disc edge. The resonances appear at the same positions, revealing that the same edge modes are excited. However, in this case the peaks are stronger and sharper. We explain the weakening and broadening of the resonances in the case of coupling with the CNT by two effects. First, the CNTPs lose energy while propagating from the exciting dipole to the disc, resulting in reduced peak heights. Second, the edge plasmons in the disc couple back to the CNT. The resonating edge plasmons thus experience additional losses, resulting in a broadening of the resonance, i.e., reduction of the quality factor.

Another interesting observation is the difference between the spatial distribution of |**E**| in the disc excited by the dipole and that of the disc excited by the CNTP (see insets to Figure 4b). While the CNTP can couple only to the clockwise propagating edge plasmon of the disc, the dipole launches both clockwise and counterclockwise plasmons. The last circumstance explains the presence of the interference fringes in the map of |**E**| for the case of the dipole excitation.

The comparison of the two configurations shows that the direct dipole excitation of a disc resonator is more efficient than its coupling to CNTPs. Nevertheless, the plasmonic resonances in the CNT−disc configuration are still visible and can be improved for graphene structures of higher quality, so that in the future this geometry might become useful for graphene-plasmonic filtering in network applications.

To complete the consideration of potential hybrid CNT−graphene disc devices, we consider a configuration having both input and output bus waveguides (which could be helpful in cases where routing of various frequencies to different output ports is needed). A structure consisting of two CNTs and a graphene disc between them is sketched in Figure 4a (right). The plasmon launched in nanotube A (input waveguide) by a vertical dipole, located in the same way as in Figure 4b, travels toward the graphene disc resonator and excites the edge GPs. The excited cavity modes then couple to the plasmon in nanotube B (output bus waveguide) so that it propagates in the opposite direction compared to the plasmon in nanotube A. The absorption both inside the disc (blue curve) and in the nanotube B (green curve) is shown in Figure 4d as a function of λ. Now the plasmonic power losses are redistributed between the disc and nanotube B so that their sum (green and blue curves in Figure 4d) is approximately the same as the losses in

DOI: 10.1021/ph500377u
ACS Photonics XXXX, XXX, XXX−XXX

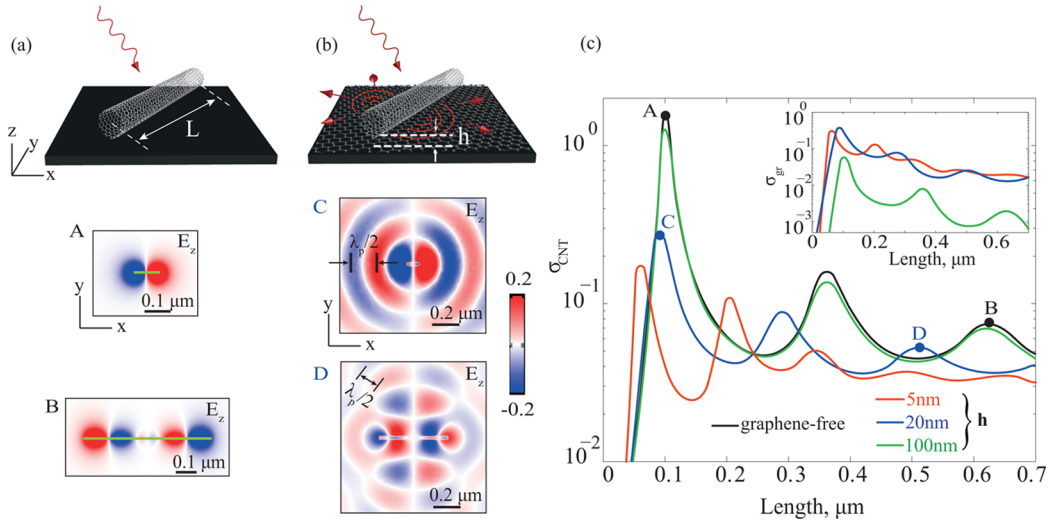

Figure 5. Plasmonic resonances in finite-length CNTs above a graphene surface. (a) Schematic and spatial distribution of Re(E_z) for the CNT without graphene corresponding to points A and B of the black curve in panel (c). (b) Schematic and spatial distribution of Re(E_z) for the CNT over graphene (h = 5 nm) at resonant peaks C and D of the black curve in panel (c). In both (a) and (b) the plane, where the fields are shown, corresponds to a constant coordinate z at which the CNT is cut in the middle. The fields are normalized to |**E**| of the incident wave. The free-space wavelength is 10 μm. (c) Absorption cross-section of CNT, σ_{CNT}, as a function of the CNT length, L, for different separation distances h. Black curve corresponds to CNT in free space. Inset to (c): Absorption cross-section of GPs, σ_{gr} (CNT-induced absorption in graphene), as a function of L. The parameters of the conductivity are the same as in Figure 1.

the disc without nanotube B (blue curve in Figure 4b). As a result, the considered device can transfer the CNTP from the incoming port into the output port for a set of resonant wavelengths with the efficiency basically determined by the intrinsic absorption of both the graphene disc and the CNTs.

Having considered the manipulation of the plasmons in CNTs with lengths much larger than the plasmon wavelength, we proceed with the demonstration of the plasmonic functionality of short CNTs. Taking into account a high figure of merit of CNTPs, a finite-length CNT can act as a subwavelength IR antenna.[22,38−42] To show the response of such an antenna, a finite-length CNT is illuminated by a normally incident plane wave with the electric field parallel to the axis of the CNT (see schematics in Figure 5a). Figure 5c (black curve) represents the normalized absorption cross-section $\sigma_{CNT} = A_{CNT}/(I_0 S_{CNT})$ of the CNT antenna as a function of CNT length L. Here A_{CNT} is the power absorbed in the CNT (which we assume to be dominated by CNTPs), I_0 is the illuminating power per unit area, and $S_{CNT} = dL$ is the geometrical CNT cross-section. A set of antenna resonances corresponding to an integer number of plasmon half-wavelengths along the CNT antenna is observed. The field distribution at the peak values of σ_{CNT} (instant snapshots of Re(E_z) in Figure 5a) reveals both the fundamental dipolar resonance (see image A, with the near fields of opposite polarity at the CNT extremities) and higher-order resonances, e.g., shown in image B.

As we have demonstrated in Figure 2a, CNTPs are sensitive to the refractive index of the substrate. We now study how the presence of a graphene sheet affects the antenna resonances in CNTs (schematics in Figure 5b). As shown in Figure 5c (red, blue, and green curves), the presence of the graphene layer below the CNT blue-shifts and broadens (damps) the resonances. The closer the CNT is to the graphene sheet, the larger the blue-shift and damping experienced. Notice that a similar resonance shift has been studied for the case of metallic antennas loaded by graphene.[29,43−47] The shift is mainly associated with the coupling of the antenna to the GPs. In our case the excitation of GPs is clearly seen from the oscillating structure of the near-fields shown in Figure 5b, where the distance between the fringes of the same color yields the GP wavelength. In an earlier work,[48] CNTs have already been shown to launch propagating plasmons on metallic surfaces in the visible spectral regime. In metals, however, the plasmons have much lower momenta than in graphene, and therefore the launching of GPs is much more difficult. Actually, an efficient excitation of propagating plasmons in graphene is still an open question.[29,32] Due to the huge momentum mismatch between the waves in free space and GPs, coupling is only possible when high-intensity near-fields are created by couplers having momenta in their Fourier spectrum that are increased by orders of magnitude relative to the incident wavevector.[1,2,29] Since a CNT antenna fulfills these two criteria, it can be utilized to launch GPs. In order to characterize the losses (dominated by the propagating plasmons) in the graphene sheet induced by a CNT, we calculate the normalized absorption cross-section for GPs according to $\sigma_{gr} = (A_{gr} - A_{gr0})/(I_0 S_{CNT})$, where A_{gr} and A_{gr0} is the absorption in the graphene sheet with and without the CNT above it, respectively. In the inset to Figure 5c we show σ_{gr} as a function of λ for different heights of the CNT above the graphene sheet, h. For all values of h the positions of the maxima for σ_{gr} coincide with those for σ_{CNT}. The cross-section σ_{gr} shows a nonmonotonic behavior with h (for h < 100 nm), so that at different wavelengths there is a height providing the best coupling between CNTPs and GPs. Further increase of h leads to a progressive decrease of σ_{gr} owing to the finite confinement length L_z of both CNTP and GP. For instance, the wavelength of GP at λ = 10 μm is λ_p = 338 nm, yielding $L_z = \lambda_p/2\pi \approx 54$ nm. Thus, for a separation of 100 nm, the absorption by the CNT is virtually nonsensitive to the presence of graphene (compare green and black curves in Figure 5c), and σ_{gr} is low so that GPs are virtually not excited (the green curve in the inset to Figure 5c). Interestingly, the phase of the field of the launched GPs is flipped with respect to that of the

DOI: 10.1021/ph500377u
ACS Photonics XXXX, XXX, XXX−XXX

CNT antenna. Since the initial phase of GPs is opposite that of the CNT antenna, the field pattern essentially depends upon the resonance order and thus can be controlled by the length of the CNT and the wavelength of the incident radiation.

One should note that the launching efficiency of the propagating GPs by CNTs is 1 order of magnitude lower than that by resonant metallic antennas[29] (found by the comparison of σ_{gr} in the inset of Figure 5c with the results of ref 29). It can be explained by the huge geometric difference of a CNT and a metal antenna (the cross-sections are 0.002 versus 2 μm^2 in the resonance, respectively) compared to the plasmon wavelength λ_p. This last difference reduces the GP launching efficiency by CNTs, but can be beneficial for the compactness of plasmonic devices. On the other hand, the efficiency can be significantly improved by creating periodic arrays of CNTs due to constructive interference between the launched GPs.

To conclude, cylindrical 2D materials have the ability to guide low-loss plasmons with ultrashort wavelength. For this reason, they can be used as promising building blocks for many plasmonic applications, especially for miniaturized photonic circuits. Compared to 2D sheets and ribbons, they offer a higher field confinement and longer propagation length and do not have edges, avoiding thus additional loss mechanisms. We have illustrated the functionalities of several plasmonic devices based on carbon nanotubes and hybrid nanotube−graphene structures: coupled waveguides, split-ring resonator, and nanotube antenna launcher. Our results promise plasmons in cylindrical 2D materials as a versatile concept for deeply subwavelength optical circuitry.

Although all the results have been achieved on the example of CNTs, they can be directly applied to other types of single-walled plasmonic/polaritonic nanotubes, in which due to thin walls their optical properties can be described by a 2D conductivity (for instance single-walled BN nanotubes[49] or semiconductor nanotubes with the walls of a nanometric thickness[50]).

METHODS

In the electromagnetic calculations, we treat all graphene and nanotube structures as infinitesimally thin objects with the following conductivity: $\sigma = ie^2|E_F|/\pi\hbar^2(\omega + i\tau^{-1})$, where E_F is the Fermi level, ω is the frequency, and τ is the scattering time of charge carriers. This model takes into account only intraband electronic transitions and ignores the temperature, which is justified for our range of parameters. The calculations have been performed with the help of the finite elements methods using Comsol software, where the monolayer structures are defined as surface currents within the boundary conditions, $\mathbf{j}_{\|} = \sigma\mathbf{E}_{\|}$, where the symbol "$\|$" means the component perpendicular to the normal vector of the surface. All the structures are discretized with a fine mesh, having the element sizes not exceeding 1/20 of the minimal local spatial oscillation period of the electromagnetic fields. This minimal period corresponds to plasmon wavelength on the CNT and graphene disc and free-space wavelength in the air and substrate.

ASSOCIATED CONTENT

Supporting Information

The Supporting Information includes additional simulations for two structures: the pair of coupled nanotubes and the nanotube coupled to the graphene disc. It also contains the discussion on a possible fabrication procedure of our plasmonic circuits. This material is available free of charge via the Internet at http://pubs.acs.org.

AUTHOR INFORMATION

Corresponding Author

*E-mail: a.nikitin@nanogune.eu.

Notes

The authors declare no competing financial interest.

ACKNOWLEDGMENTS

This work was financially supported by the European Commission under Graphene Flagship (contract no. CNECT-ICT-604391) and the Spanish Ministry of Economy and Competitiveness (National Projects MAT2012-36580).

REFERENCES

(1) Chen, J.; Badioli, M.; Alonso-Gonzalez, P.; Thongrattanasiri, S.; Huth, F.; Osmond, J.; Spasenovic, M.; Centeno, A.; Pesquera, A.; Godignon, P.; Zurutuza Elorza, A.; Camara, N.; de Abajo, F. J. G.; Hillenbrand, R.; Koppens, F. H. L. Optical nano-imaging of gate-tunable graphene plasmons. *Nature* **2012**, *487*, 77−81.

(2) Fei, Z.; Rodin, A. S.; Andreev, G. O.; Bao, W.; McLeod, A. S.; Wagner, M.; Zhang, L. M.; Zhao, Z.; Thiemens, M.; Dominguez, G.; Fogler, M. M.; Neto, A. H. C.; Lau, C. N.; Keilmann, F.; Basov, D. N. Gate-tuning of graphene plasmons revealed by infrared nano-imaging. *Nature* **2012**, *487*, 82−85.

(3) Grigorenko, A. N.; Polini, M.; Novoselov, K. S. Graphene plasmonics. *Nat. Photonics* **2012**, *6*, 749−758.

(4) Hanson, G. W. Dyadic Green's functions and guided surface waves for a surface conductivity model of graphene. *J. Appl. Phys.* **2008**, *103*, 064302.

(5) Jablan, M.; Buljan, H.; Soljačić, M. Plasmonics in graphene at infrared frequencies. *Phys. Rev. B* **2009**, *80*, 245435.

(6) Koppens, F. H. L.; Chang, D. E.; García de Abaj, F. J. Graphene plasmonics: a platform for strong light−matter interactions. *Nano Lett.* **2011**, *11*, 3370−3377.

(7) Nikitin, A. Y.; Guinea, F.; Garcia-Vidal, F. J.; Martin-Moreno, L. Fields radiated by a nanoemitter in a graphene sheet. *Phys. Rev. B* **2011**, *84*, 195446.

(8) Vakil, A.; Engheta, N. Transformation optics using graphene. *Science* **2011**, *332*, 1291−1294.

(9) Wunsch, B.; Stauber, T.; Sols, F.; Guinea, F. Dynamical polarization of graphene at finite doping. *New J. Phys.* **2006**, *8*, 318.

(10) García de Abajo, F. J. Graphene plasmonics: challenges and opportunities. *ACS Photonics* **2014**, *1*, 135−152.

(11) Fang, Z.; Thongrattanasiri, S.; Schlather, A.; Liu, Z.; Ma, L.; Wang, Y.; Ajayan, P. M.; Nordlander, P.; Halas, N. J.; García de Abajo, F. J. Gated tunability and hybridization of localized plasmons in nanostructured graphene. *ACS Nano* **2013**, *7*, 2388−2395.

(12) Francescato, Y.; Giannini, V.; Yang, J.; Huang, M.; Maier, S. A. Graphene sandwiches as a platform for broadband molecular spectroscopy. *ACS Photonics* **2014**, *1*, 437−443.

(13) Nikitin, A. Y.; Guinea, F.; García-Vidal, F. J.; Martín-Moreno, L. Edge and waveguide terahertz surface plasmon modes in graphene microribbons. *Phys. Rev. B* **2011**, *84*, 161407.

(14) Yan, H.; Low, T.; Zhu, W.; Wu, Y.; Freitag, M.; Li, X.; Guinea, F.; Avouris, P.; Xia, F. Damping pathways of mid-infrared plasmons in graphene nanostructures. *Nat. Photonics* **2013**, *7*, 394−399.

(15) Charlier, J.-C.; Blase, X.; Roche, S. Electronic and transport properties of nanotubes. *Rev. Mod. Phys.* **2007**, *79*, 677−732.

(16) Avouris, P.; Freitag, M.; Perebeinos, V. Carbon-nanotube photonics and optoelectronics. *Nat. Photonics* **2008**, *2*, 341−350.

(17) Gao, Y.; Ren, G.; Zhu, B.; Liu, H.; Lian, Y.; Jian, S. Analytical model for plasmon modes in graphene-coated nanowire. *Opt. Express* **2014**, *22*, 24322−24331.

(18) Lin, M. F.; Shung, K. W. K. Elementary excitations in cylindrical tubules. *Phys. Rev. B* **1993**, *47*, 6617−6624.

DOI: 10.1021/ph500377u
ACS Photonics XXXX, XXX, XXX−XXX

(19) Longe, P.; Bose, S. M. Collective excitations in metallic graphene tubules. *Phys. Rev. B* **1993**, *48*, 18239−18243.
(20) Jiang, X. Collective plasmon excitations in graphene tubules. *Phys. Rev. B* **1996**, *54*, 13487−13490.
(21) Moradi, A. Coupled Surface Plasmon-polariton modes of metallic single-walled carbon nanotubes. *Plasmonics* **2013**, *8*, 1509−1513.
(22) Zhang, Q.; Hároz, E. H.; Jin, Z.; Ren, L.; Wang, X.; Arvidson, R. S.; Lüttge, A.; Kono, J. Plasmonic nature of the terahertz conductivity peak in single-wall carbon nanotubes. *Nano Lett.* **2013**, *13*, 5991−5996.
(23) Falkovsky, L. A. Optical properties of graphene and IV−VI semiconductors. *Phys.-Usp.* **2008**, *51*, 887−897.
(24) Hwang, E. H.; Das Sarma, S. Dielectric function, screening, and plasmons in two-dimensional graphene. *Phys. Rev. B* **2007**, *75*, 205418.
(25) Queipo, P.; Nasibulin, A. G.; Shandakov, S. D.; Jiang, H.; Gonzalez, D.; Kauppinen, E. I. CVD synthesis and radial deformations of large diameter single-walled CNTs. *Curr. Appl. Phys.* **2009**, *9*, 301−305.
(26) Ma, J.; Wang, J. N.; Wang, X. X. Large-diameter and water-dispersible single-walled carbon nanotubes: synthesis, characterization and applications. *J. Mater. Chem.* **2009**, *19*, 3033−3041.
(27) Jeong, G.-H.; Suzuki, S.; Kobayashi, Y.; Yamazaki, A.; Yoshimura, H.; Homma, Y. Effect of nanoparticle density on narrow diameter distribution of carbon nanotubes and particle evolution during chemical vapor deposition growth. *J. Appl. Phys.* **2005**, *98*, 124311.
(28) Kobayashi, K.; Kitaura, R.; Nishimura, F.; Yoshikawa, H.; Awaga, K.; Shinohara, H. Growth of large-diameter (∼4 nm) single-wall carbon nanotubes in the nanospace of mesoporous material SBA-15. *Carbon* **2011**, *49*, 5173−5179.
(29) Alonso-González, P.; Nikitin, A. Y.; Golmar, F.; Centeno, A.; Pesquera, A.; Vélez, S.; Chen, J.; Navickaite, G.; Koppens, F.; Zurutuza, A.; Casanova, F.; Hueso, L. E.; Hillenbrand, R. Controlling graphene plasmons with resonant metal antennas and spatial conductivity patterns. *Science* **2014**, *344*, 1369−1373.
(30) The momentum of a plasmon is complex-valued. For simplicity, throughout the text and in the figures, if we do not explicitly mention the compexity of the mometum, we imply only its real part.
(31) Nesterov, M. L.; Kats, A. V.; Turitsyn, S. K. Extremely short-length surface plasmon resonance devices. *Opt. Express* **2008**, *16*, 20227−20240.
(32) Nikitin, A. Y.; Alonso-González, P.; Hillenbrand, R. Efficient coupling of light to graphene plasmons by compressing surface polaritons with tapered bulk materials. *Nano Lett.* **2014**, *14*, 2896−2901.
(33) Yariv, A. *Quantum Electronics*; John Wiley & Sons: New York, 1975.
(34) Gumbs, G.; Balassis, A. Effects of coupling on plasmon modes and drift-induced instabilities in a pair of cylindrical nanotubes. *Phys. Rev. B* **2003**, *68*, 075405.
(35) Moradi, A. Plasma wave propagation in a pair of carbon nanotubes. *JETP Lett.* **2008**, *88*, 795−798.
(36) Bozhevolnyi, S. I.; Volkov, V. S.; Devaux, E.; Laluet, J.-Y.; Ebbesen, T. W. Channel plasmon subwavelength waveguide components including interferometers and ring resonators. *Nature* **2006**, *440*, 508−511.
(37) Martin-Cano, D.; Nesterov, M. L.; Fernandez-Dominguez, A. I.; Garcia-Vidal, F. J.; Martin-Moreno, L.; Moreno, E. Domino plasmons for subwavelengthterahertz circuitry. *Opt. Express* **2010**, *18*, 754−764.
(38) Jeon, T.-I.; Kim, K.-J.; Kang, C.; Oh, S.-J.; Son, J.-H.; An, K. H.; Bae, D. J.; Lee, Y. H. Terahertz conductivity of anisotropic single walled carbon nanotube films. *Appl. Phys. Lett.* **2002**, *80*, 3403−3405.
(39) Akima, N.; Iwasa, Y.; Brown, S.; Barbour, A. M.; Cao, J.; Musfeldt, J. L.; Matsui, H.; Toyota, N.; Shiraishi, M.; Shimoda, H.; Zhou, O. Strong anisotropy in the far-infrared absorption spectra of stretch-aligned single-walled carbon nanotubes. *Adv. Mater.* **2006**, *18*, 1166−1169.
(40) Slepyan, G. Y.; Shuba, M. V.; Maksimenko, S. A.; Thomsen, C.; Lakhtakia, A. Terahertz conductivity peak in composite materials containing carbon nanotubes: theory and interpretation of experiment. *Phys. Rev. B* **2010**, *81*, 205423.
(41) Shuba, M. V.; Paddubskaya, A. G.; Plyushch, A. O.; Kuzhir, P. P.; Slepyan, G. Y.; Maksimenko, S. A.; Ksenevich, V. K.; Buka, P.; Seliuta, D.; Kasalynas, I.; Macutkevic, J.; Valusis, G.; Thomsen, C.; Lakhtakia, A. Experimental evidence of localized plasmon resonance in composite materials containing single-wall carbon nanotubes. *Phys. Rev. B* **2012**, *85*, 165435.
(42) Nakanishi, T.; Ando, T. Optical response of finite-length carbon nanotubes. *J. Phys. Soc. Jpn.* **2009**, *78*, 114708.
(43) Fang, Z.; Wang, Y.; Liu, Z.; Schlather, A.; Ajayan, P. M.; Koppens, F. H. L.; Nordlander, P.; Halas, N. J. Plasmon-induced doping of graphene. *ACS Nano* **2012**, *6*, 10222−10228.
(44) Yao, Y.; Kats, M. A.; Genevet, P.; Yu, N.; Song, Y.; Kong, J.; Capasso, F. Broad electrical tuning of graphene-loaded plasmonic antennas. *Nano Lett.* **2013**, *13*, 1257−1264.
(45) Emani, N. K.; Chung, T.-F.; Ni, X.; Kildishev, A. V.; Chen, Y. P.; Boltasseva, A. Electrically tunable damping of plasmonic resonances with graphene. *Nano Lett.* **2012**, *12*, 5202−5206.
(46) Mousavi, S. H.; Kholmanov, I.; Alici, K. B.; Purtseladze, D.; Arju, N.; Tatar, K.; Fozdar, D. Y.; Suk, J. W.; Hao, Y.; Khanikaev, A. B.; Ruoff, R. S.; Shvets, G. Inductive tuning of Fano-resonant metasurfaces using plasmonic response of graphene in the mid-infrared. *Nano Lett.* **2013**, *13*, 1111−1117.
(47) Emani, N. K.; Chung, T.-F.; Kildishev, A. V.; Shalaev, V. M.; Chen, Y. P.; Boltasseva, A. Electrical modulation of Fano resonance in plasmonic nanostructures using graphene. *Nano Lett.* **2013**, *14*, 78−82.
(48) Hartmann, N.; Piredda, G.; Berthelot, J.; Colas des Francs, G.; Bouhelier, A.; Hartschuh, A. Launching propagating surface plasmon polaritons by a single carbon nanotube dipolar emitter. *Nano Lett.* **2011**, *12*, 177−181.
(49) Xu, X. G.; Ghamsari, B. G.; Jiang, J.-H.; Gilburd, L.; Andreev, G. O.; Zhi, C.; Bando, Y.; Golberg, D.; Berini, P.; Walker, G. C. One-dimensional surface phonon polaritons in boron nitride nanotubes. *Nat. Commun.* **2014**, *5*.
(50) Yusheng, B.; Zheng, Z.; Xin, Z.; Yalin, S.; Lei, L.; Jiansheng, L.; Tao, Z.; Jinsong, Z. Hybrid plasmonic structures based on CdS nanotubes: a novel route to low-threshold lasing on the nanoscale. *J. Phys. D: Appl. Phys.* **2012**, *45*, 505105.

DOI: 10.1021/ph500377u
ACS Photonics XXXX, XXX, XXX−XXX